Front. Phys., 2014, 9(6): 760–767
DOI 10.1007/s11467-014-0441-1

RESEARCH ARTICLE

A computational investigation of topological insulator Bi_2Se_3 film

Yi-Bin Hu[1], **Yong-Hong Zhao**[2], **Xue-Feng Wang**[3]

[1] *Department of Physics, McGill University, 3600 rue University, Montréal, Québec, H3A 2T8, Canada*

[2] *College of Physics and Electronic Engineering, Institute of Solid State Physics, Sichuan Normal University, Chengdu 610068, China*

[3] *Department of Physics, Soochow University, Suzhou 215006, China*

Corresponding author. E-mail: †*huy@physics.mcgill.ca*

Received April 16, 2014; accepted June 28, 2014

Topological insulators have a bulk band gap like an ordinary insulator and conducting states on their edge or surface which are formed by spin–orbit coupling and protected by time-reversal symmetry. We report theoretical analyses of the electronic properties of three-dimensional topological insulator Bi_2Se_3 film on different energies. We choose five different energies (–123, –75, 0, 180, 350 meV) around the Dirac cone (–113 meV). When energy is close to the Dirac cone, the properties of wave function match the topological insulator's hallmark perfectly. When energy is far way from the Dirac cone, the hallmark of topological insulator is broken and the helical states disappear. The electronic properties of helical states are dug out from the calculation results. The spin-momentum locking of the helical states are confirmed. A 3-fold symmetry of the helical states in Brillouin zone is also revealed. The penetration depth of the helical states is two quintuple layers which can be identified from layer projection. The charge contribution on each quintuple layer depends on the energy, and has completely different behavior along K and M direction in Brillouin zone. From orbital projection, we can find that the maximum charge contribution of the helical states is p_z orbit and the charge contribution on p_y and p_x orbits have 2-fold symmetry.

Keywords topological insulator, spin–orbit coupling, helical state

PACS numbers 73.20.-r

Frontiers of Physics

1 Introduction

The idea of topological insulator has attracted tremendous attention recently [1–8]. The topological insulator is an insulator that has metallic edge states when it is placed to a vaccum. These metallic edge states originate from topological invariants. These topological edge states in the topological insulator have opposite spin polarization when their momentums are along opposite direction. These topological edge states are induced by spin-orbit coupling and protected by the time-reversal symmetry. It is locked between the electron spin polarization and the electron momentum. For these topological edge states, spin cannot be flipped and backscattering should be suppressed, if the time-reversal symmetry can preserve. The topological insulators have significant applied potential in nanoelectronics due to their peculiar transport properties.

Bi_2Se_3 is a typical three-dimensional topological insulator material. This material has stacked quasi-two-dimentional layer structure named quintuple layer (QL) which contains five atomic layers (Se-Bi-Se-Bi-Se). Each QL is stable and hard to break due to the strong interactions between atoms therein. But the interaction between QLs are very weak. There are metallic helical states on the edges of topological insulator Bi_2Se_3 film. A Dirac cone which is a characteristic signature of topological insulator has been observed in Bi_2Se_3 film by studying the surface band structure with ARPES and first-principles calculations [9]. Concurrent theoretical work also has been done by using electronic structure methods to show that Bi_2Se_3 is just one of large band-gap topological insulators. A simple tight-binding model is provided to get the Dirac cone observed in these materials [10]. Some other experimental investigations of Bi_2Se_3 surface can be found in the literatures [11–15]. For theoretical investigations, there are two main methods, one is model

hamiltonian [16], the other is first-principles calculation [17]. The first method is based on the physical picture of topological insulators, and an effective Hamiltonian is derived for the topological surface states. The second method is based on first-principles calculation, and electronic structure of the topological surface states can be calculated. There are several focuses of the topological surface states' investigations now. They are new materials prediction [9, 10, 18], material properties [11, 12, 15, 19–21], doping properties [13, 14, 22, 23], etc.

In this paper, we investigate the helical states of Bi_2Se_3 film from ab initio calculation completely and reveal the characteristic signature of Bi_2Se_3 film from the atomic wave function without any phenomenological parameter. In compare to our previous work [21], we optimize the basis set of Bi and Se elements. This basis set is smaller, but closer to the benckmark band structure which is simulated by WIEN2k. The energy-dependent properties of the helical states which are very important for electronic transport are the focus of this paper, and these theoretical investigations are absent. From the calculation results, we can find the energy range where helical states exist and electronic properties' difference between different energies which can be used to predict the transport behavior of electronic devices based on Bi_2Se_3 film. Compare to the corresponding experimental data, we confirm several very important electronic properties of topological insulator Bi_2Se_3 film. We also predict some interesting phenomenons which may be validated by other experiments.

2 Electronic structure of the Bi_2Se_3 film

All of the relaxation processes are done by the full-potential linearly augmented plane waves method as implemented in the WIEN2k electronic simulation package [24]. For lattice relaxation, we use the primitive cell of Bi_2Se_3 crystal. In the LAPW method, the unit cell is divided into two parts — non-overlapping atomic spheres and interstitial region. The non-overlapping atomic spheres for Bi_2Se_3 crystal are set to $R_{\mathrm{MT}} = 2.0$ Bohr. The maximum angular momentum for the spherical harmonics expansion inside the atomic spheres was taken to be $l_{\max} = 10$. The plane wave expansion in the interstitial region was determinated by a cutoff parameter $RK_{\max} = 8.0$. A k-point mesh of $10 \times 10 \times 10$ is employed for k-sampling. The optimized lattice vectors of the Bi_2Se_3 crystal are found to be $a = 4.107$ Å and $c = 27.89$ Å. They agree well with the experimental values of 4.138 Å and 28.64 Å, respectively [17]. Then we use slab model to simulate two dimentional structure. In the slab model, the Bi_2Se_3 film contains six QLs and there is a vacuum of 20 Å thickness between the Bi_2Se_3 films. In the slab calculation, the parameters R_{MT}, $l_{\max}$ and $RK_{\max}$ are same with the bulk calculation, and k-point mesh is changed to $20 \times 20 \times 1$. The atomic structure of Bi_2Se_3 film is considered fully relaxed until the force on each atom is smaller than 1 mRy/Bohr.

Using the relaxed atomic structure, we calculate the electronic properties of the Bi_2Se_3 film by WIEN2k and nanodcal [25, 26]. In WIEN2k, R_{MT} is changed to 2.4 Bohr, other parameters are same with the relaxation calculation. In nanodcal, a linear combination of atomic orbital (LCAO) method is used to expand physical quantities, the standard norm-conserving pseudopotentials [27] are used to define the atomic core states, the spin–orbit coupling is handled at the atomic level [28, 29], and the noncollinear spin capability of nanodcal is ideal for analyzing the helical states. The local spin density approximation (LSDA) [30] is used for the exchange-correlation potential in all the calculations. In our previous work [21], we use a triple-ζ polarization LCAO basis set (TZDP). Now we use different basis sets for surface atoms and bulk atoms. This is a very effective method which only needs a double-ζ polarization LCAO basis set (DZP) for each atom. A k-point mesh of $20 \times 20 \times 1$ is employed for k-sampling, and the energy cutoff for the real space grid is taken as 600 Ry. Self-consistent calculation is considered converged until each element of the density matrix is converged to less than 10^{-5} au.

The calculated band structure of the Bi_2Se_3 film is shown in Fig. 1. The red curve is the band structure calculated by nanodcal. The blue curve is the band structure calculated by WIEN2k. Because the atomic orbital is not a complete basis set, it is hard to reproduce all the features presented in the WIEN2k results. We focus on how to decrease the integral error of band strustruce when tuning the pseudopotentials and atomic orbitals. And a reasonable band structure of the Bi_2Se_3 film is achived. A Dirac cone is clearly formed around the Γ point of the Brillouin zone due to strong spin–orbit coupling, which is one of most important characteristics of three dimentional topological insulators. For the Bi_2Se_3 film, the calculated Fermi level E_f is ~113 meV above the Dirac cone, and the helical states are around the Dirac cone. So we choose several typical energies around the Dirac cone to investigate the physical properties of these helical states. From Kohn–Sham equation, we can obtain wavefunction of these typical helical states. After that, we calculate spin polarization vector to check spin-momentum locking, layer contribution to reveal penetration depth, and orbital contribution to find components of the helical states.

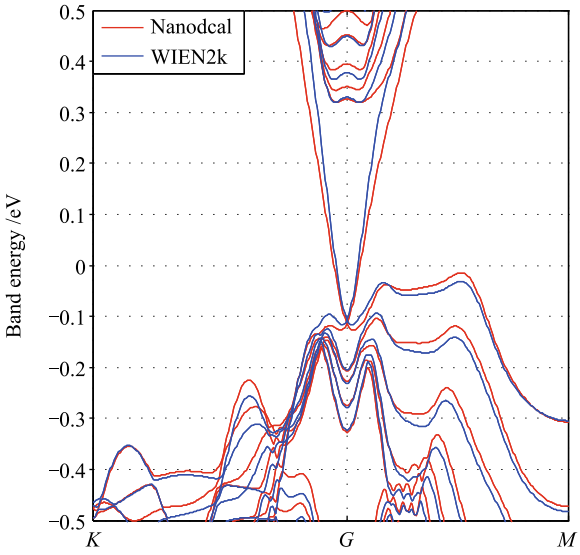

Fig. 1 Calculated band structure of the Bi_2Se_3 film: the red curve is calculated by nanodcal; the blue curve is calculated by WIEN2k.

3 Spin-momentum locking of the Bi_2Se_3 film

Due to spin–orbit coupling, the electronic structure of the Bi_2Se_3 film must be analyzed with noncollinear spin whose wavefunction is two-component spinors $|\psi_{nk}\rangle = (|\psi_{nk}^{\uparrow}\rangle, |\psi_{nk}^{\downarrow}\rangle)$, where n is the band index and k is the Bloch wave vector index. We construct the k-space density matrix from the noncollinear spin wavefunction,

$$\hat{\rho}_{nk} = |\psi_{nk}\rangle\langle\psi_{nk}| = \begin{pmatrix} |\psi_{nk}^{\uparrow}\rangle\langle\psi_{nk}^{\uparrow}| & |\psi_{nk}^{\uparrow}\rangle\langle\psi_{nk}^{\downarrow}| \\ |\psi_{nk}^{\downarrow}\rangle\langle\psi_{nk}^{\uparrow}| & |\psi_{nk}^{\downarrow}\rangle\langle\psi_{nk}^{\downarrow}| \end{pmatrix} \quad (1)$$

From the above k-space density matrix, we can calculate the charge contribution straightforwardly,

$$\hat{Q}_{nk} = \frac{\hat{\rho}_{nk}\hat{s}_k + \hat{s}_k\hat{\rho}_{nk}}{2} = \frac{1}{2}\mathrm{Tr}\begin{pmatrix} \rho_{nk}^{\uparrow\uparrow}s_k + s_k\rho_{nk}^{\uparrow\uparrow} & \rho_{nk}^{\uparrow\downarrow}s_k + s_k\rho_{nk}^{\uparrow\downarrow} \\ \rho_{nk}^{\downarrow\uparrow}s_k + s_k\rho_{nk}^{\downarrow\uparrow} & \rho_{nk}^{\downarrow\downarrow}s_k + s_k\rho_{nk}^{\downarrow\downarrow} \end{pmatrix} \quad (2)$$

where s_k is the k-space overlap matrix of atomic orbits due to nonorthogonal basis used in the calculation. Because the system is analyzed with noncollinear spin, the form of charge contribution is 2 by 2 matrix. This charge contribution can be further decomposed with the Pauli matrix $\hat{\sigma}$,

$$\hat{Q}_{nk} = q\hat{I} + p_x\hat{\sigma_x} + p_y\hat{\sigma_y} + p_z\hat{\sigma_z} \quad (3)$$

where q is the charge contribution, $\boldsymbol{p} = (p_x, p_y, p_z)$ is the spin polarization vector.

For convenience, we define five variables to identify position and spin polarization vector of helical state [see Fig. 2(a)]. The length R defines the distance from Γ to helical state in k-space. The angle θ defines the azimuth angle of helical state, zero degree point to the high symmetry point M in k-space, anticlockwise direction is positive. These two variables identify position of helical state. The polarization S defines the quantity of spin polarization vector $(\rho_\uparrow - \rho_\downarrow)/(\rho_\uparrow + \rho_\downarrow)$. The azimuth angle Ψ and the tilting angle Φ define the direction of spin polarization vector. For the azimuth angle Ψ, zero degree point to the extention from Γ to helical state, anticlockwise direction is positive. For the tilting angle Φ, zero degree means spin polarization vector is parallel to the surface of the Bi_2Se_3 film, it is positive when p_z is larger than zero. These three variables identify spin polarization vector of helical state.

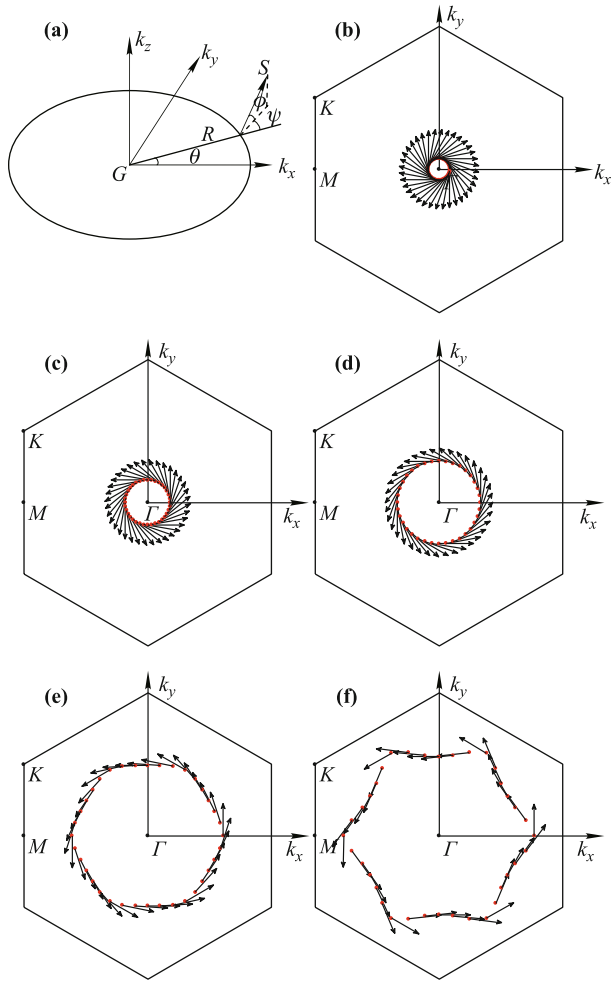

Fig. 2 **(a)** define five variables to identify helical state and spin polarization vector: length R, angle θ, polarization S, azimuth angle Ψ and tilting angle Φ. (b–f) is the diagram of spin polarization vector projected in two-dimensional plane. The red dot means helical state, the black arrow means spin polarization vector. **(b)** $E = -123$ meV, the shape is a circle. **(c)** $E = -75$ meV, the shape is a circle. **(d)** $E = 0$ meV, the shape is almost a circle. **(e)** $E = 180$ meV, the shape is a hexagon. **(f)** $E = 350$ meV, the shape is a hexagram.

We investigate the helical states at five different ener-

gies. These energies are –123, –75, 0 (Fermi level), 180, 350 meV. Because the shape of these helical states for a certain energy is a closed curve around Γ point, we select helical state each 10 degree along the angle θ. There are totally 36 samples for each energy. There are two identical surfaces (top and bottom) in the Bi_2Se_3 film, hence two degenerate helical states are found at each k-point. We calculate wavefunction of these helical states and analyze their spin polarization vectors. We find two degenerate helical states are symmetrical completely, spin polarization is zero if we add the spin polarization vector of two degenerate helical states together. So we only show the calculation result of one degenerate helical state which locates in the bottom surface of the Bi_2Se_3 film.

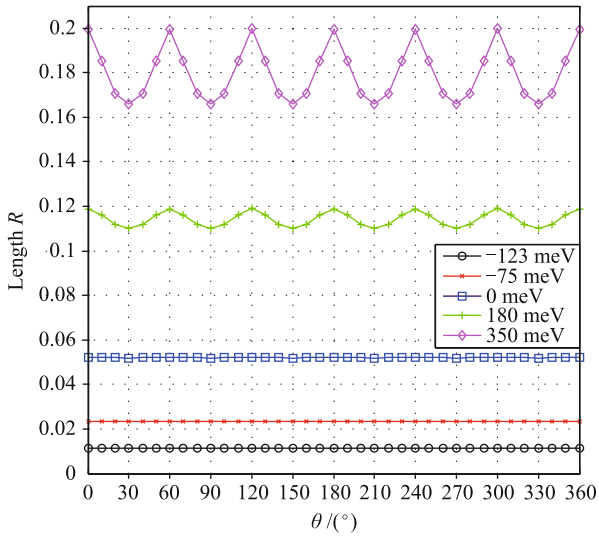

Fig. 3 The length R of the helical states versus the angle θ for five different energies.

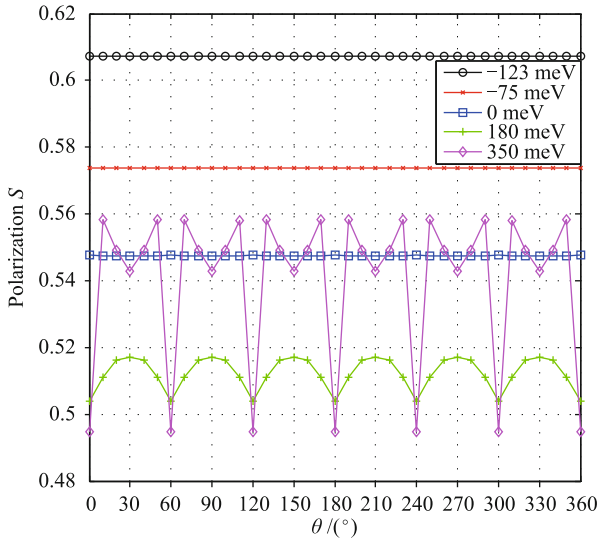

Fig. 4 The polarization S of the helical states versus the angle θ for five different energies.

Figure 3 shows the relation between length R and angle θ for different energies. Figure 4 shows the relation between polarization S and angle θ for different energies. Figure 5 shows the relation between the azimuth angle Ψ of spin polarization vector and angle θ for different energies. Figure 6 shows the relation between the tilting angle Φ of spin polarization vector and angle θ for different energies. Figures 2(b)–(f) show the diagram of spin polarization vectors in different energies projected in two-dimensional plane which is parallel to the surface of the Bi_2Se_3 film. In the diagram, the red dot means helical state, black arrow means spin polarization vector.

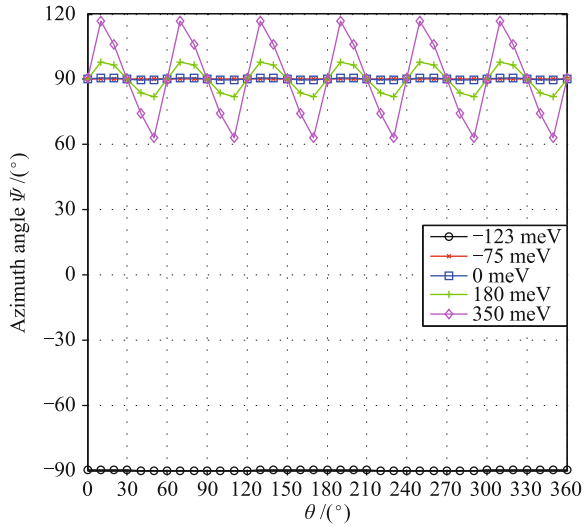

Fig. 5 The azimuth angle Ψ of the helical states versus the angle θ for five different energies.

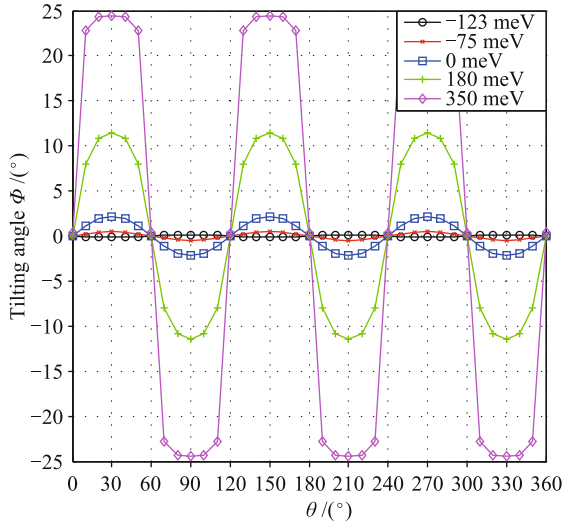

Fig. 6 The tilting angle Φ of the helical states versus the angle θ for five different energies.

From Fig. 3, the length R is constant when energy is –123 and –75 meV which means the shape of helical state

is a circle [see Figs. 2(b) and (c)]; the length R has a tiny oscillation when energy is 0 meV which means the shape of helical state is almost a circle [see Fig. 2(d)]; the length R has a large oscillation when energy is 180 meV, the maximum length R is along M direction, the minimum length R is along K direction, the shape of helical state is a hexagon [see Fig. 2(e)]; the length R has a huge oscillation when energy is 350 meV, the maximum length R is along M direction, the minimum length R is along K direction, the shape of helical state is a hexagram [see Fig. 2(f)]. We find that the length R for specified energy have a 6-fold symmetry and the shape is closer to circle when energy is closer to the Dirac cone. This interesting phenomenon can also be reported in the experiment [3, 20].

The behavior of polarization S is similar to length R. From Fig. 4, we can find the helical states are highly ploarized in k-space, but it is not 100% polarized, consistent with previous result [19]. The spin polarization is around 0.607 when energy is –123 meV. The spin polarization is around 0.574 when energy is –75 meV. For energy is 0 meV, the spin polarization is around 0.547 and there is a tiny oscillation. For energy is 180 meV, the spin polarization has a large oscillation, the maximum spin polarization is around K direction and the minimum spin polarization is along M direction. For energy is 350 meV, the spin polarization has a huge oscillation, the spin polarization around K and M direction is a local minimum.

The spin-momentum locking can be clearly revealed by Fig. 5. For energy is –123 meV, the azimuth angle Ψ is –90 degree ($-90° \pm 0.003°$). For energy is –75 meV, the azimuth angle Ψ is 90 degree ($90° \pm 0.02°$). These results mean the spin polarization vector is vertical to momentum. And we can also find the spin polarization vector is clockwise for –123 meV which is below Dirac cone, but the spin polarization vector is anticlockwise for –75 meV which is above Dirac cone. Figures 2(b) and (c) show the diagram respectively. These properties match the topological insulator's hallmark ($\boldsymbol{P}(+\boldsymbol{k}) = -\boldsymbol{P}(-\boldsymbol{k})$) perfectly. For energy is 0 meV, the azimuth angle Ψ is $90° \pm 0.5°$. For energy is 180 meV, the azimuth angle Ψ is $90° \pm 8°$. For energy is 350 meV, the azimuth angle Ψ is $90° \pm 27°$. For these helical states, the spin polarization vector is not vertical to momentum exactly, but the spin polarization vector has almost opposite direction at $+\boldsymbol{k}$ and $-\boldsymbol{k}$ ($\boldsymbol{P}(+\boldsymbol{k}) \approx -\boldsymbol{P}(-\boldsymbol{k})$). The spin-momentum locking is still established, but not perfect. Figures 2(d), (e) and (f) show the diagram respectively. The spin polarization vector is anticlockwise and the direction of spin polarization vector is almost along the tangent of helical state's shape.

Interestingly and quantitatively, the spin polarization vector is found to not completely lie in the two dimentional Brillouin zone plane from Fig. 6. We can find a period of 120° for the titling angle Φ, which reflects 3-fold rotational symmetry of the Bi_2Se_3 film (space group D^5_{3d}). The maximum value of $|\Phi|$ is 0.15° for –123 meV, 0.48° for –75 meV, 2.2° for 0 meV, 12° for 180 meV, 25° for 350 meV. A tilting angle of 5° at Fermi level is reported experimentally [13] which is consistant with our calculation results.

4 Layer projection of the Bi_2Se_3 film

For investigating how the helical states distributes in the Bi_2Se_3 film, we calculate charge projection on each QL for these helical states. Figure 7 shows layer contribution of the helical states along K direction, Fig. 8 shows layer contribution of the helical states along M direction. These two direction are most important in the Brillouin zone, the behavior of other directions are similar.

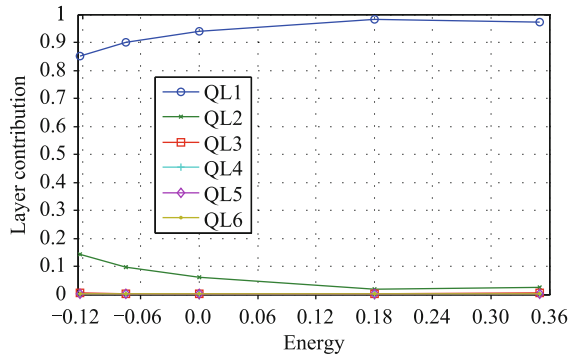

Fig. 7 The layer contribution on different QLs along K direction. Six different curves mean six different QLs from bottom to top.

When energy is –123, –75, 0 meV, the layer contribution of the helical states is same and independent on the direction mainly. The layer contribution for first two QLs are around 99%. These results can identify that the helical states are surface states and two degenerate helical states are separated in real space. When energy is 180, 350 meV, the layer contribution of the helical states depends on the direction (see Figs. 7 and 8). We can find that the behavior of the layer contribution along K and M direction is different completely. The helical states along K direction are still surface states like those helical states in lower energies (–123, –75, 0 meV). But the helical states along M direction is entirely unexpected. The layer contribution for first two QLs decreases to around 97% (for 180 meV) and 67% (for 350 meV). This is a downward tendency obviously. These helical states cannot be regarded as surface states.

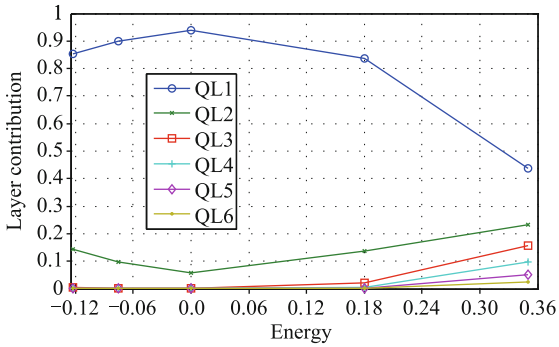

Fig. 8 The layer contribution on different QLs along M direction. Six different curves mean six different QLs from bottom to top.

5 Orbital projection of the Bi_2Se_3 film

For investigating the components of the helical states in the Bi_2Se_3 film, we calculate charge projection on each orbit of each atom for these helical states. Because the helical states match the hallmark of topological insulator only when energy is close to Dirac cone (–113 meV). So we only analyze first QL's orbital contribution of these helical states at Fermi level (0 meV).

From the calculation results, the charge contribution on d orbits is very small. So in Fig. 9, we only plot charge contribution on s, p orbits. The charge contribution on first QL at Fermi level is around 94%. The charge contribution on s, p_z orbits are almost independent on the angle θ. The most important is p_z orbit, the charge contribution is around 42%. The charge contribution on s orbit is around 6%. The charge contribution on p_y, p_x orbits depend on the angle θ, and have a period of 180°. The largest value of the charge contribution on p_y and p_x orbits are along y and x axis respectively. There is an interesting thing that the sum of the charge contribution on p_y and p_x orbits is around 42%.

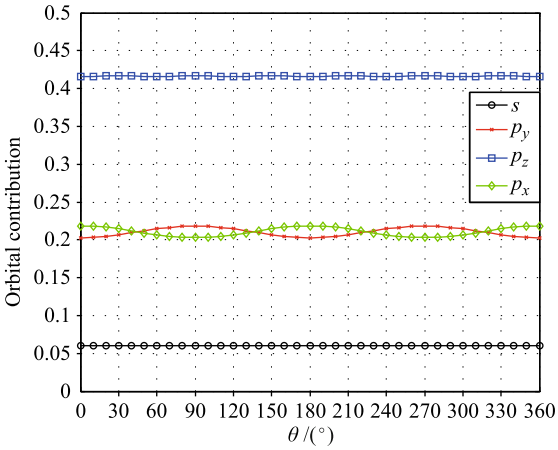

Fig. 9 The orbital contribution on the first QLs at Fermi level. Because the d orbit's charge contribution are very small, we plot s, p_y, p_z, p_x orbit's charge contribution only.

From the orbital contribution on each atomic layer, the charge contribution on p_z orbit comes from Bi atomic layers mainly, and the charge contribution on s orbit comes from Se atomic layers mainly. The most interesting thing comes from p_y and p_x orbits. Figure 10 shows the p_y orbit's layer contribution on different atomic layers in the first QL. The p_y orbit's charge contribution on Bi atomic layers are ordinary, and only have a tiny oscillation. The p_y orbit's charge contribution on Se atomic layers are unexpected. They depend on the angle θ, and has a period of 180°. The largest and smallest value of the p_y orbit's charge contribution on the first atomic layer (Se) is along x and y axis respectively. But the largest and smallest value of the p_y orbit's charge contribution on the third and fifth atomic layer (Se) are along y and x axis respectively. The properties are opposite between the first atomic layer (Se) and the third (fifth) atomic layer (Se). The symmetry of p_y orbit's charge contribution on the first QL is determined by the third and fifth atomic layer (Se) which is different with the first atomic layer (Se). Figure 11 shows the p_x orbit's layer contribution on different atomic layers in the first QL. For p_x orbit, the behavior is similar to p_y orbit.

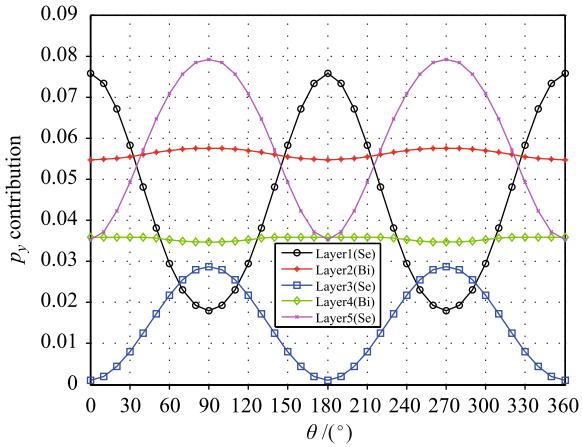

Fig. 10 The p_y orbit's charge contribution on different atomic layers in the first QL at Fermi level. Five different curves mean five different atomic layers in the first QL from surface to base.

6 Summary

For the Bi_2Se_3 film, we have calculated physical properties of the helical states at five different energies (–123, –75, 0, 180, 350 meV) self-consistently without any phenomenological parameter. The band structure has a Dirac cone (–113 meV) at Γ due to spin–orbit coupling.

There are helical states in the Bi_2Se_3 film when

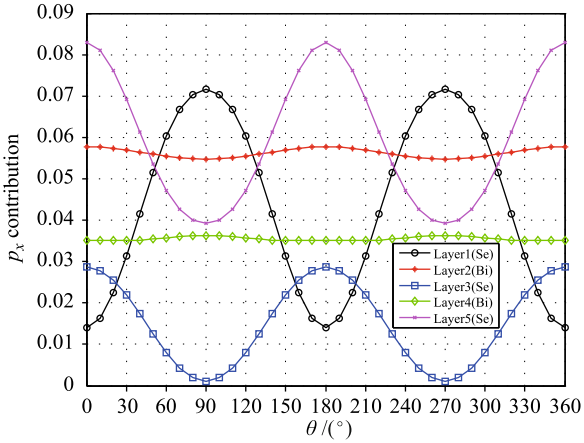

Fig. 11 The p_x orbit's charge contribution on different atomic layers in the first QL at Fermi level. Five different curves mean five different atomic layers in the first QL from surface to base.

energy is close to the Dirac cone (–123, –75, 0 meV). These states have following features: the shape of states is a circle; the state is a surface state; the spin-momentum locking is well established. All these features are the characteristic signatures of topological insulators and the electron's backscattering is suppressed. When energy is far from the Dirac cone (180, 350 meV), the physical properties of states are dependent on the direction. The shape of states is a hexagon for 180 meV, a hexagram for 350 meV. The states along K direction are still helical states, similar with those states in lower energies (–123, –75, 0 meV). But for the states along M direction, the physical properties are different, and the above features are destroyed. The state spreads over the Bi_2Se_3 film entirely, and it is not a surface state. It is not orthogonal between the spin and momentum of states, and the spin-momentum locking is not perfect. The electron's backscattering cannot be suppressed, and the transport behavior must be ordinary.

The orbital contribution on each atomic layer of the helical states are calculated. The maximum charge contribution comes from the p_z orbit, others comes from s, p_y, p_x orbits. The charge contribution on p_z, s orbits are almost independent on the angle θ. There is 2-fold symmetry in the charge contribution on p_y, p_x orbits. There is an interesting phenomenon that the charge contribution on p_y, p_x orbits in the first atomic layer (Se) has different symmetry with the charge contribution on p_y, p_x orbits in the first QL.

Acknowledgements We would like to thank Hong Guo for discussion, and thank Lei Liu and Eric Zhu for assistance in numerical calculations using the nanodcal software. Yong-Hong Zhao is supported by the National Natural Science Foundation of China (Grant No. 11104191). Xue-Feng Wang is supported by the National Natural Science Foundation of China (Grant Nos. 11074182 and 91121021). We gratefully acknowledge RQCHP and CLUMEQ for computing facilities.

References and notes

1. C. L. Kane and E. J. Mele, Z_2 topological order and the quantum spin Hall effect, *Phys. Rev. Lett.*, 2005, 95(14): 146802
2. B. A. Bernevig, T. L. Hughes, and S. C. Zhang, Quantum spin Hall effect and topological phase transition in HgTe quantum wells, *Science*, 2006, 314(5806): 1757
3. M. Z. Hasan and C. L. Kane, Colloquium: Topological insulators, *Rev. Mod. Phys.*, 2010, 82(4): 3045
4. X. L. Qi and S. C. Zhang, Topological insulators and superconductors, *Rev. Mod. Phys.*, 2011, 83(4): 1057
5. X. L. Qi and S. C. Zhang, The quantum spin Hall effect and topological insulators, *Phys. Today*, 2010, 63(1): 33
6. J. E. Moore, The birth of topological insulators, *Nature*, 2010, 464(7286): 194
7. L. Fu and C. L. Kane, Topological insulators with inversion symmetry, *Phys. Rev. B*, 2007, 76(4): 045302
8. X. L. Qi, T. L. Hughes, and S. C. Zhang, Topological field theory of time-reversal invariant insulators, *Phys. Rev. B*, 2008, 78(19): 195424
9. Y. Xia, D. Qian, D. Hsieh, L. Wray, A. Pal, H. Lin, A. Bansil, D. Grauer, Y. S. Hor, R. J. Cava, and M. Z. Hasan, Observation of a large-gap topological-insulator class with a single Dirac cone on the surface, *Nat. Phys.*, 2009, 5(6): 398
10. H. J. Zhang, C. X. Liu, X. L. Qi, X. Dai, Z. Fang, and S. C. Zhang, Topological insulators in Bi_2Se_3, Bi_2Te_3 and Sb_2Te_3 with a single Dirac cone on the surface, *Nat. Phys.*, 2009, 5(6): 438
11. D. Hsieh, Y. Xia, D. Qian, L. Wray, F. Meier, J. H. Dil, J. Osterwalder, L. Patthey, A. V. Fedorov, H. Lin, A. Bansil, D. Grauer, Y. S. Hor, R. J. Cava, and M. Z. Hasan, Observation of time-reversal-protected single-Dirac-cone topological-insulator states in Bi_2Te_3 and Sb_2Te_3, *Phys. Rev. Lett.*, 2009, 103(14): 146401
12. K. He, Y. Zhang, K. He, C. Z. Chang, C. L. Song, L. L. Wang, X. Chen, J. F. Jia, Z. Fang, X. Dai, W. Y. Shan, S. Q. Shen, Q. Niu, X. L. Qi, S. C. Zhang, X. C. Ma, and Q. K. Xue, Crossover of the three-dimensional topological insulator Bi_2Se_3 to the two-dimensional limit, *Nat. Phys.*, 2010, 6(8): 584
13. D. Hsieh, Y. Xia, D. Qian, L. Wray, J. H. Dil, F. Meier, J. Osterwalder, L. Patthey, J. G. Checkelsky, N. P. Ong, A. V. Fedorov, H. Lin, A. Bansil, D. Grauer, Y. S. Hor, R. J. Cava, and M. Z. Hasan, A tunable topological insulator in the spin helical Dirac transport regime, *Nature*, 2009, 460(7259): 1101
14. Y. S. Hor, A. Richardella, P. Roushan, Y. Xia, J. G. Checkelsky, A. Yazdani, M. Z. Hasan, N. P. Ong, and R. J. Cava, p-type Bi_2Se_3 for topological insulator and low-temperature

thermoelectric applications, *Phys. Rev. B*, 2009, 79(19): 195208

15. S. R. Park, W. S. Jung, C. Kim, D. J. Song, C. Kim, S. Kimura, K. D. Lee, and N. Hur, Quasiparticle scattering and the protected nature of the topological states in a parent topological insulator Bi_2Se_3, *Phys. Rev. B*, 2010, 81: 041405(R)
16. C. X. Liu, X. L. Qi, H. J. Zhang, X. Dai, Z. Fang, and S. C. Zhang, Model Hamiltonian for topological insulators, *Phys. Rev. B*, 2010, 82(4): 045122
17. W. Zhang, R. Yu, S. J. Zhang, X. Dai, and Z. Fang, First-principles studies of the three-dimensional strong topological insulators Bi_2Te_3, Bi_2Se_3 and Sb_2Te_3, *New J. Phys.*, 2010, 12(6): 065013
18. Jeongwoo Kim, Jinwoong Kim, and Seung-Hoon Jhi, Prediction of topological insulating behavior in crystalline Ge-Sb-Te, *Phys. Rev. B*, 2010, 82: 201312(R)
19. O. V. Yazyev, J. E. Moore, and S. G. Louie, Spin polarization and transport of surface states in the topological insulators Bi_2Se_3 and Bi_2Te_3 from first principles, *Phys. Rev. Lett.*, 2010, 105(26): 266806
20. Z. Alpichshev, J. G. Analytis, J.-H. Chu, I. R. Fisher, Y. L. Chen, Z. X. Shen, A. Fang, and A. Kapitulnik, STM imaging of electronic waves on the surface of Bi_2Te_3: Topologically protected surface states and hexagonal warping effects, *Phys. Rev. Lett.*, 2010, 104(1): 016401
21. Y. H. Zhao, Y. B. Hu, L. Liu, Y. Zhu, and H. Guo, Helical states of topological insulator Bi_2Se_3, *Nano Lett.*, 2011, 11(5): 2088
22. R. Yu, W. Zhang, H. J. Zhang, S. C. Zhang, X. Dai, and Z. Fang, Quantized anomalous Hall effect in magnetic topological insulators, *Science*, 2010, 329(5987): 61
23. T. M. Schmidt, R. H. Miwa, and A. Fazzio, Spin texture and magnetic anisotropy of Co impurities in Bi_2Se_3 topological insulators, *Phys. Rev. B*, 2011, 84(24): 245418
24. P. Blaha, K. Schwarz, P. Sorantin, and S. B. Trickey, Full-potential, linearized augmented plane wave programs for crystalline systems, *Comput. Phys. Commun.*, 1990, 59(2): 399
25. Nanodcal is developed by NanoAcademic Technologies Inc. (http://www.nanoacademic.ca/) Nanodcal is an LCAO implementation of density functional theory within the Keldysh nonequilibrium Greens function formalism. It is a general purpose tool for ab initio modeling of electronic structure, equilibrium and non-equilibrium quantum transport.
26. J. Taylor, H. Guo, and J. Wang, Ab initio modeling of quantum transport properties of molecular electronic devices, *Phys. Rev. B*, 2001, 63(24): 245407
27. L. Kleinman and D. M. Bylander, Efficacious form for model pseudopotentials, *Phys. Rev. Lett.*, 1982, 48(20): 1425
28. G. Theurich and N. A. Hill, Self-consistent treatment of spin-orbit coupling in solids using relativistic fully separable ab initio pseudopotentials, *Phys. Rev. B*, 2001, 64(7): 073106
29. L. Fernández-Seivane, M. A. Oliveria, S. Sanvito, and J. Ferrer, On-site approximation for spin–orbit coupling in linear combination of atomic orbitals density functional methods, *J. Phys.: Condens. Matter*, 2006, 18(34): 7999
30. J. P. Perdew and Y. Wang, Accurate and simple analytic representation of the electron-gas correlation energy, *Phys. Rev. B*, 1992, 45(23): 13244